THE
PHYSICAL REVIEW

A journal of experimental and theoretical physics established by E. L. Nichols in 1893

SECOND SERIES, VOL. 75, No. 3 FEBRUARY 1, 1949

Experiments on *N–P* Scattering with 90- and 40-Mev Neutrons*

J. HADLEY, E. KELLY, C. LEITH, E. SEGRÈ, C. WIEGAND, AND H. YORK
Radiation Laboratory, Department of Physics, University of California, Berkeley, California

(Received October 25, 1948)

In this paper we describe some measurements of the neutron-proton scattering cross section at neutron energies of approximately 40 and 90 Mev. Both the total scattering cross section and the differential cross section as a function of the angle of scattering were measured.

I. INTRODUCTION

ONE of the important experiments that became feasible as soon as the 184-inch cyclotron started to operate was an investigation of the *n-p* scattering at a neutron energy around 90 Mev. As is well known, *n-p* scattering at high energy may yield interesting clues to the nuclear forces and data on it constitute important experimental material against which any future theory must be checked. The investigation acquires particular important if the De Broglie wave-length of the neutron in the center of gravity system (c.g. system) is comparable with the range of nuclear forces. The De Broglie wavelength is given by

$$\lambda\!\!\!^{-} = \hbar/p = 9.0\times10^{-13}/E^{\frac{1}{2}} \text{ cm}.$$

(E in Mev in laboratory system; p = reduced mass × relative *n-p* velocity) and in the region of $E=100$ Mev has a value favorable for investigating *n-p* scattering. Neutrons of this energy are produced when the deuterons of the cyclotron are stripped in collision with nuclei of the target. A beam of neutrons of small, angular aperture and of fairly narrow energy distribution results.[1,2] This energy distribution has a maximum at about 90 Mev ($\lambda\!\!\!^{-}=0.95\times10^{-13}$ cm).

In the investigation to be described we have studied (*a*) the angular dependence of the scattering cross section, (*b*) the total cross section[3] at neutron energies of 90 Mev and 40 Mev. The angular measurements were extended over scattering angles in the c.g. system from 36 to 180 degrees.

To avoid unnecessary repetitions we shall now define the angles used in this paper (see Fig. 1). We shall call the angle of scattering of the neutron in the c.g. system θ; the angle of scattering of the neutron in the laboratory system Θ; the angle between the direction of motion of the incoming neutron and the recoil *proton* in the c.g. system and in the laboratory system, φ and Φ, respectively.

Between these angles we have the following relations:

$$\text{tg}\Theta = (1-\beta^2)^{\frac{1}{2}}\,\text{tg}(\theta/2), \tag{1}$$

$$\text{tg}\Phi = (1-\beta^2)^{\frac{1}{2}}\,\text{cotg}(\theta/2), \tag{2}$$

$$\frac{d}{d}\frac{\cos\Phi}{\cos\theta} = \frac{1}{4}\frac{1}{1-\beta^2}\frac{(1-\beta^2\cos^2\Phi)^2}{\cos\Phi}, \tag{3}$$

$$E_n = Mc^2(2\beta^2/1-\beta^2), \tag{4}$$

$$E_p = 2\beta^2Mc^2/(1-\beta^2+\text{tg}^2\Theta), \tag{5}$$

where E_n and E_p are the kinetic energies of neutron and

* A short preliminary report of this work has been given in Phys. Rev. **73**, 1114 (1948).

[1] A. C. Helmholz, E. M. McMillan, and D. Sewell, Phys. Rev. **72**, 1003 (1947).

[2] R. Serber, Phys. Rev. **72**, 1008 (1947).

[3] See also Cook, McMillan, Peterson, and Sewell, Phys. Rev. **72**, 1264 (1947).

proton in the laboratory system, M is the rest mass of proton or neutron (considered equal), and β is the ratio of the velocity of the neutron in the c.g. system to the velocity of light. In our experiments ($E_n = 88$ Mev)β is equal to 0.2124 and the relativity effects start to be visible.

The principle of our experiment is to measure the number of protons scattered from a hydrogenous target into a fixed solid angle $d\Omega = d\psi d\cos\Phi$ at angle Φ; this number is proportional to the differential cross section $\sigma(\Phi)$ and from this we find the differential cross section $\sigma(\theta) = \sigma(\Phi)(d\cos\Phi/d\cos\theta)$ in the c.g. system. The direct measurement of $\sigma(\Phi)$ is not on an *absolute* scale, but we can normalize it and pass to an absolute scale by requiring that

$$\int \sigma(\Phi) d\Omega = \text{total scattering cross section} = \sigma_t. \quad (6)$$

This last quantity is obtained by measuring the attenuation of the neutron beam in passing through suitable absorbers. In practice, polyethylene or paraffin was used and the effect of carbon was measured (using graphite) and subtracted.

The main results of the investigation are contained in Tables II, III, and IV, and in Fig. 10.

II. ANGULAR DISTRIBUTION EXPERIMENTS

A. General Description

For angles Φ between 0° and 60° we have used apparatus A and B, the general arrangement of which is shown in Fig. 2. For angles $\Phi > 55°$ we have used a different apparatus to be described later. The neutron beam coming from the cyclotron was produced by stripping 180-Mev deuterons on beryllium. It was monitored either by protons scattered from an auxiliary polyethylene target or by a bismuth fission chamber.[4]

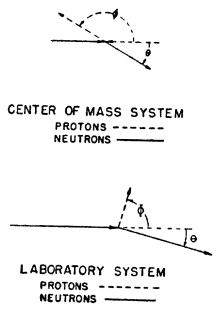

FIG. 1. Definitions of angles referred to in the text.

The scattered protons were detected by a telescope of three proportional counters pointing at the scatterer. The counter telescope was made insensitive to protons generated by primary neutrons of energy less than 66 Mev, by interposing between the last two counters an aluminum absorber (absorber A of Fig. 2) of a thickness such that it would stop all protons of an energy $< 66\cos^2\Phi$ Mev.

We measured the relative number of protons scattered by a polyethylene target per impinging neutron by registering the ratio R_1 between coincidence counts obtained in the telescope and the counts of the monitor. Subsequently the polyethylene target was replaced by a graphite target having the same stopping power for protons as the polyethylene target, and the ratio R_2 similar to R_1 was measured. Finally without any target we obtained the ratio R_3.

The effect, H, resulting from the hydrogen is obtained by

$$\begin{aligned} H &= (R_1 - R_3) - 0.713(R_2 - R_3) \\ &= R_1 - 0.713R_2 - 0.287R_3, \end{aligned} \quad (7)$$

where the coefficient 0.713 is the ratio between the number of atoms per cm² of carbon in the polyethylene target and the graphite target having the same stopping power for protons. H/t (t is the effective thickness of the target) is proportional to the cross section for n-p scattering. The statistical standard deviation of H, δH, is given by

$$[(\delta R_1)^2 + (0.713\delta R_2)^2 + (0.287\delta R_3)^2]^{\frac{1}{2}} = \delta H, \quad (8)$$

where δR_1 is the standard deviation of R_1, etc.

To fit the data obtained in different runs we proceeded as follows: Runs Nos. 1, 2, 12 (see Table II) have eight values of Φ in common. For these values the geometrical mean of the H/t values was calculated and a curve drawn. The other runs have one or more points in common with runs 1, 2, 12. These points were used to normalize the run in such a way that for the values of Φ common to the run in question and to the curve obtained from runs 1, 2, 12, the value of H/t would be the same, or, in case of more points in common, make a best fit. In doing

[4] C. Wiegand, Rev. Sci. Inst. 19, 790 (1948).

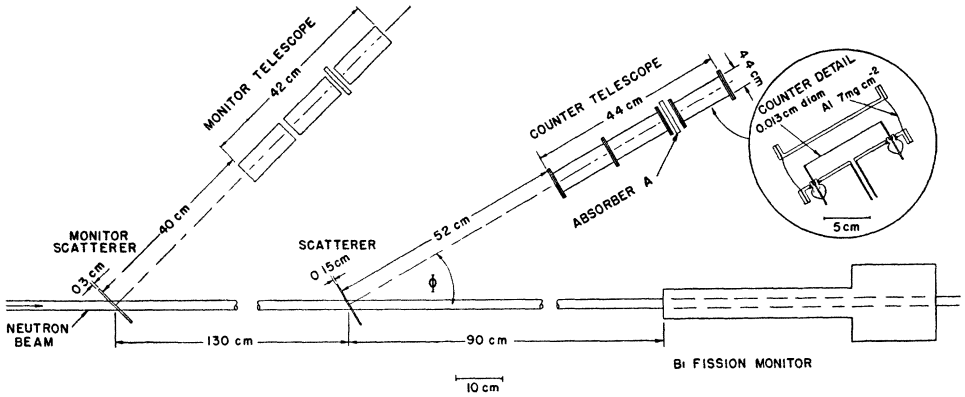

FIG. 2. General arrangement of apparatus A and B.

this we added to the statistical error of the measurement of H/t a fitting error equal to $(H/t)\times\delta\rho$, where $\delta\rho$ is the error in the normalization factor ρ. This can be estimated from the variation of ρ for various values of Φ or from the statistical errors of the single measurements. The statistical error of the single measurements and $(H/t)\delta\rho$ add by the usual rule:

$$\{[\delta(H/t)]^2+[(H/t)\delta\rho)^2]\}^{\frac{1}{2}}. \quad (9)$$

Having thus obtained H/t as a function of Φ, we have at once on a relative scale the n-p scattering cross section as a function of Φ. To show the results obtained we report in Table II the values of H/t obtained in all runs and treated as described above to bring them all to the same scale. The errors listed are the standard deviations calculated from statistics on the single measurements. No account has been taken of the effect of $\delta\rho$.

We now give details of the instruments and of the single phases of the experiment.

B. Neutron Beam

The neutron beam was produced by stripping 180-Mev deuterons on a 1.27-cm thickness of beryllium. Its average energy is about 90 Mev. The beam was collimated by a hole in the 10-foot thick concrete walls of the cyclotron shield and emerged through an aperture of a diameter that has been varied in the different experiments from 7.5 cm to 1 cm. This aperture consisted of holes in two 50-cm long copper plugs, one at each side of the concrete shield. The beam was accurately centered either by obtaining a photographic image on an x-ray film in front of which we had put some paraffin or by looking with a cathetometer at the beryllium probe in the cyclotron.

The energy distribution of the neutrons to be expected in the primary beam is given by Serber's theory.[5] It is desirable, however, to have a direct experimental confirmation of the distribution because although the excellent agreement with the angular distribution of neutrons as measured[1] is good proof of the soundness of the picture, we want to know also if there are many neutrons of lower energy arising from other effects. We have, for this reason, taken a curve of coincidence counting rate as a function of the thickness of the absorber A, keeping Φ constant at 15°. From this curve it is possible to calculate by differentiation the energy distribution of the protons passing through absorber A, and by taking into account the dependence of the np scattering cross section on energy and angle it is possible to reconstruct the energy distribution of the neutrons in the primary beam.

The same distribution has also been investigated by lowering the voltage in the counter behind absorber A in the telescope in such a way that it was sensitive only to protons near the end of their range. The results of both experiments are shown in Fig. 3 together with Serber's theoretical curve. Agreement with Serber's diagram is good for the high energy region, but we have some indications of an appreciable number of neutrons of lower energy. This subject has not been further investigated because all our detectors were operated in such a way as to be

[5] R. Serber, Phys. Rev. 72, 1008 (1947).

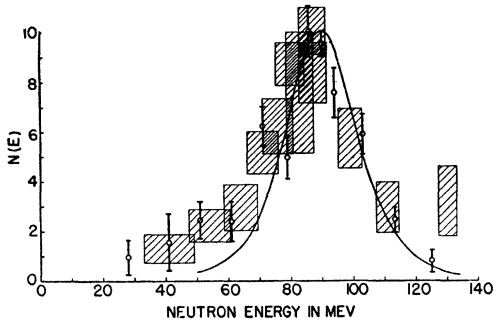

FIG. 3. Energy distribution of the primary neutrons in the beam obtained by stripping 190-Mev deuterons on 1.27-cm thick beryllium. The solid curve is from Serber's theory. The shaded rectangles are the results obtained by desensitizing the counter behind absorber A and varying the thickness of absorber A. The vertical lines are the results obtained by variation of absorber A and differentiation of the curve of absorber thickness *versus* number of coincidences.

insensitive to protons generated by primary neutrons of energy lower than 66 Mev. The cloud-chamber group[6] has obtained very good histograms of the energy of the neutrons in the primary beam showing agreement with Serber's theory.

At 45 Mev we do not have direct data on the energy distribution of the neutrons in the primary beam and we have assumed that Serber's theory gives the correct distribution.

C. Detecting Telescope

The scattered protons were detected with a telescope of three proportional counters pointing at the scatterer. The counters were brass cylinders 5 cm in diameter, about 13 cm long, with a 5-mil wire on the axis, filled at atmospheric pressure with a mixture of argon and carbon dioxide in the ratio 25 to 1 by volume. The front windows were 45 mg cm^{-2} copper or 7 mg cm^{-2} aluminum.

As we have already said, the telescope was made insensitive to protons generated by primary neutrons having an energy smaller than 66 Mev by interposing between the last two counters an aluminum absorber (absorber A of Fig. 2) of a thickness such that it would stop all protons of an energy smaller than 66 Mev $\cos^2\Phi$. More precisely, the absorber A placed in the coincidence telescope was chosen so that the minimum energy a neutron must have in order to give a detectable scattered proton was 66 Mev, if the proton was generated in an infinitesimal layer at half the depth of the scatterer. The energy loss of the protons in the scatterer makes this condition only approximate for other layers of a thick scatterer, and since the thickness of the scatterer in terms of energy loss becomes greater as Φ increases, the error increases with Φ. However, even in the case of the widest angles measured, a neutron must have (66+7) Mev in order to give a detectable proton from the side of the scatterer farther from the detector, and (66−7) Mev if it originates from the side nearer to the detector. The neutron energy distribution as measured by us, when multiplied by $\sigma(E)\simeq(A/E)$, shows that the correction necessitated by the effect of the thickness of the scatterer is negligible (±2 percent) because the number of protons originating at the far side of the scatterer and lost by absorption is almost exactly compensated by the excess of low energy protons originating at the near side of the scatterer.

At the neutron energies used in this experiment, the absorbers A are so thick (several grams/cm^2) that some protons which would otherwise pass through are removed either by Rutherford scattering or nuclear absorption. For apparatus A, where the absorber was placed immediately in front of the last counter, Rutherford scattering was negligible, and only the nuclear absorption produced any effect.

In apparatus C (see Section F and Fig. 7) it was necessary to place the absorber in front of all three counters. In the experimental arrangement, about one-half of the protons scattered by more than 3° would not be counted by the coincidence counter telescope. The fraction of protons lost due to this scattering is proportional to $N\sigma_\alpha$, where N is the number of atoms per cm^2 in the absorber, of atomic number Z, and σ_α is the cross section of the absorber for Rutherford scattering through an angle greater than α. σ_α is proportional to $Z/\alpha^2E_p^2$ and since at each angle Φ, N is varied approximately proportionately to E_p^2, the fraction of protons lost is nearly independent of Φ. To check this point and to find out what fraction was lost, we counted the number of protons going through various absorbers with the same stopping power but with differing Z. For this purpose C, Al, Cu, and Pb

[6] K. Bruckner, W. Hartsough, E. Hayward, and W. Powell; to be submitted to Phys. Rev.

were used. By plotting counting rate *versus* NZ^2/E_p^2, and extrapolating to $Z=0$, we found that at $\Phi=10°$, 45°, and 65° the fraction lost was about constant and equal to 4 percent for carbon, which was the absorber actually used with apparatus *C*. At the largest angle used, there was no carbon absorber in front of the counters, the principal part of the absorber being the gas in the counters themselves. Any Rutherford scattering which occurred would have taken place in the counters, and essentially no protons would have been lost due to this effect. Therefore, a correction of -4 percent has been applied to the value of $\sigma(\Phi)$ at 71.6° in order to be consistent with the rest of the data.

An estimate of nuclear scattering and absorption, originating from nuclear interaction, by the absorber *A* shows that it will not exceed about 4 percent in the worst conditions. Moreover, the difference between the magnitude of these effects at various angles is about half the absolute value. For this reason this effect has been neglected.

The amplifiers were conventional ones with times of rise varying from 0.2 microsecond in some of the sets to 0.5 microsecond in others. The scaling circuits were also quite conventional and allowed the recording of individual counts in each of the counter tubes. The coincidence circuits were of two types: In one model delay lines were used to obtain the gate-open times; in the other model multivibrators were used to form the gates. Gate times varied from about 0.5 to 12 microseconds and will be discussed in Section E.

D. Geometry and Scatterer

The approximate angular resolution of our apparatus was given by the diameter d of the counter furthest from the scatterer divided by its distance D from the scatterer, i.e., 2/50 radians. Since the scatterer itself was extended, the resolution was perhaps 3°. If one wishes to take into account the error in $\sigma(\Phi)$ introduced by the imperfect resolution, it is easily shown that the finite resolving power introduces a negligible correction unless the curve has very sharp irregularities. Only near $\Phi=0°$ may this correction be of any significance; at that point we estimate that it will raise the true cross section above the observed one by at least 10^{-27} cm^2 (7 percent) for the 90-Mev case and not appreciably affect it in the 40-Mev case.

The scattering targets were always very thin to neutrons; their thickness was determined by consideration of the energy lost in the scattering target by scattered protons. The target was always kept perpendicular to the direction of the telescope. The neutrons thus traversed an effective target thickness t equal to $s/\cos\Phi$, where s is the true target thickness. At constant beam, the number of neutrons crossing the target per unit time multiplied by the effective target thickness was independent of Φ if the beam always filled the whole scatterer, because on varying Φ the change of effective area was exactly compensated by the change of effective thickness. On the other hand, if the beam was smaller than the target area, the number of neutrons crossing the target per unit time multiplied by the effective target thickness was proportional to $s/\cos\Phi$. Both modes of operation were used. The detecting telescope could always see the whole scattering target.

E. Tests on the Apparatus and Typical Performance

It was necessary to ascertain that we counted all the protons of energy larger than 66 Mev $\cos^2\Phi$ coming from the target and nothing else. For this purpose we first studied the counter response *versus* voltage. With the telescope set at 10°, in order to be dealing with protons of practically maximum energy and hence minimum specific ionization, the coincidence counting rate *versus* the collection voltage of the counters was measured. Plateaus extending over about 300 volts were quite readily obtainable as shown in

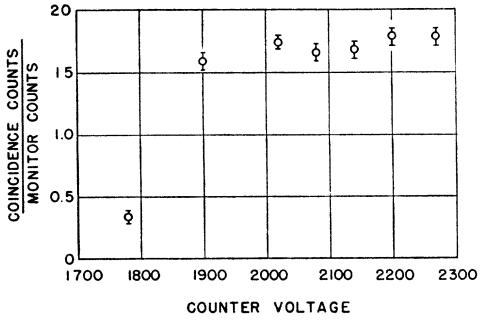

FIG. 4. Typical voltage plateau of counters.

TABLE I. Typical data.

Counter voltage	Angle Φ deg.	R*	Time sec.	Counts in each tube No. 1	No. 2	No. 3	Coinc. counts	Monitor counts	Coinc. mon.	Absorber mg cm^{-2} Al	Scatterer mg cm^{-2}
2200 volts	10	2	200	40200	43000	42400	995	1559	0.638±0.03	3857	CH_2 150
2080	10	2	200	27800	28600	28800	1007	1523	0.662±0.03	3857	CH_2 150
1960	10	2	200	14400	12800	13100	685	1118	0.613±0.03	3857	CH_2 150
2120	10	2	600	46400	46600	47600	1560	2309	0.676±0.02	3857	CH_2 150
2120	10	2	200	15600	17300	16600	232	768	0.302±0.02	3857	C 182
2120	10	2	200	14600	13800	15900	114	795	0.143±0.01$_4$	3857	blank
2120	45	2	600	45200	42600	41600	499	2106	0.237±0.01	900	CH_2 150
2120	45	2	200	17900	16900	16100	126	1017	0.124±0.01	900	C 182
2120	45	2	110	10500	9720	9720	20	636	0.031±0.01	900	blank

Notes.—*R** is the reading of a "radiation" meter near the yoke of the cyclotron magnet. It is just a check on the operation of the cyclotron and not suitable as a beam monitor.
The first three readings were taken to check the counter voltage *vs.* coincidence/monitor plateau.
The results of the above two runs give: $H_{10°}=0.420\pm0.03$, $H_{45°}=0.139\pm0.01_4$.

Fig. 4. When the counters were adjusted to detect protons of 100-Mev energy, we found that the counters were also sensitive to the recoil electrons produced when a source of radium was brought near the counter. This was to be expected on the basis of the ionization produced by high energy protons and the ionization made by electrons. The sensitivity to these electrons provided a means of rough preliminary adjustment of the counters. Although the voltage plateau would indicate that all of the protons were being counted, more certainty can be obtained from the following experiment: With the counters in operation at a fixed angle, e.g., 10°, the triple coincidence counting ratio R_1 was obtained. Then the middle counter was disconnected (this procedure leaves the geometry unchanged) and a double coincidence count was obtained with the first and third counters in coincidence. If the number of protons recorded from the scatterer is the same as with the triple coincidence set-up, we feel justified in assuming that the efficiency is practically 100 percent,

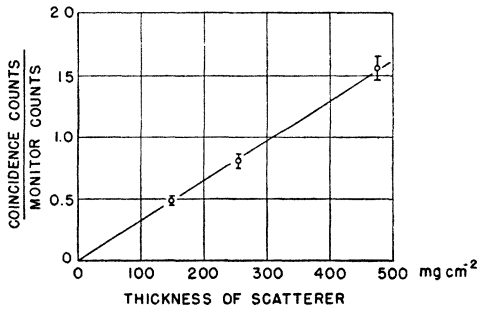

FIG. 5. Coincidence counts *versus* thickness of scatterer.

because if it were not, the use of only two counters would increase the number of coincidences obtained. A similar experiment was also done using four counters in coincidence and only the suppression of the counter farthest from the target, which obviously changes the geometry, had any effect on R_1. The reason for using triple coincidence rather than double coincidence is that a better radio of R_1 to R_3 is obtained, and that accidental coincidences are practically zero.

Another test is to determine the accidental coincidences. This was done by again setting the telescope at 10°, and obtaining the triple coincidence ratio R_1. Then the middle counter was removed physically from the telescope and placed just adjacent to its regular position. In this position the coincidence counts were reduced by a factor of about 1000, showing that the accidental coincidences were negligible. This is what one should expect if the apparatus were working properly. It is easy to overload the counters because of the fact that the neutrons are emitted by the cyclotron in short bursts. The last test described shows conclusively that this is not the case because spurious coincidences, which are unaffected if we put the counters out of line with the target, were not present. This point was further confirmed by showing that H/t was independent of the target thickness t and of the beam intensity in the region of operation, as shown in Fig. 5.

Experiments on the counting of protons with various gate times of the coincidence circuits showed that approximately the same counting efficiency was obtained with gate widths from

TABLE II. 90-Mev $\sigma(\Phi)$ in 10^{-27} cm^2 per steradian. All runs have been fitted to the average of runs 1, 2, and 12.

Run number	1	2	3	4	5	6	7	8	9	10	11	12		
Symbol in Fig.	○	●	△	×	□	▽	▭	▲	▯	▽	□	○		
Date	2-4-48	2-9-48	2-19-48	3-18-48	5-21-48	6-17-48	7-29-48	3-23-48	4-10-48	4-21-48	5-10-48	6-2-48		
Apparatus	*A*	*A*	*A*	*A*	*A*	*A*	*A*	*C*	*C*	*C*	*C*	*B*		
Φ(degrees)													θ(degrees)	$\frac{d\cos\Phi}{d\cos\theta}$
0						68.6±4.9	61.3±3.6						180.0	0.239
2				56.4±5.6									175.9	0.239
3				55.5±4.0	53.6±1.2								173.9	0.239
5	49.6±3.8	50.8±5.6		58.2±4.0	50.9±1.6								169.8	0.240
7												46.4±1.8	165.7	0.241
10	42.8±3.1	50.0±4.2		41.8±1.6	43.5±1.2	47.6±1.2	45.0±2.0					44.9±1.1	159.5	0.243
15	36.7±2.1	38.3±2.7										35.2±1.1	149.3	0.249
20	32.2±2.2	29.5±2.9				29.5±1.5						31.2±1.0	139.1	0.256
25	22.5±1.3	25.4±2.5										25.2±0.9	129.0	0.268
30	22.1±1.5	20.7±2.2										21.5±0.7	118.8	0.282
35	17.5±1.1	17.0±2.0	17.7±1.0									18.0±0.9	108.8	0.301
40	14.8±1.1	13.0±1.9										13.8±0.6	98.7	0.324
45	12.9±1.4	12.4±1.2	12.0±0.6	11.8±0.9	12.5±1.0			12.2±1.1	11.2±1.1	10.7±0.7	12.2±1.1	12.0±0.4	88.7	0.354
50	10.5±0.9	8.4±1.3											78.7	0.393
55	9.0±0.8	8.1±0.6	8.6±0.7						9.0±1.2	9.7±0.9			68.8	0.443
59		6.3±1.1											60.8	0.497
60								9.0±1.1		10.0±0.9	11.1±0.9		58.9	0.511
65									8.3±0.9	10.5±0.7			49.0	0.610
71.6								9.3±0.9	8.7±1.0	10.5±0.8	8.3±0.9		36.0	0.824

about 2 to 10 microseconds. Appropriate settings for the gate times amounted to 2 to 3 microseconds, as shown in Fig. 6.

An actual run started by a check of the gain of the amplifying systems effected by placing a radium source in a standard position with respect to the counter tubes and observing with an oscillograph the maximum height of the pulses produced by recoil electrons from the walls of the counters. This was done with a collection voltage on the counter tubes which was found to be on the plateau of the coincidence counting rate *versus* voltage curve of the previous run. The observed pulses were synchronized one on top of the other so that the pulse shape was shown. Pulses from the three proportional counter tubes were checked to make sure that the rise and decay times, respectively, were approximately equal in the three counters. These were rather qualitative checks but were capable of showing immediately any large changes in the characteristics of the counting system. A standard size pulse was applied in turn to the inputs of each of the scaling circuits to check that the minimum pulse height to trip the discriminators had not changed. The coincidence circuit gate length was checked on a calibrated sweep.

The measurements for different Φ in a single run were alternated so as to minimize possible trends in systematic errors, e.g., the following order was used in a run: $\Phi=10°$, 45°, 30°, 20°, 50°, 15°, 40°, 25°, 35°, 5°, 55° (February 4, 1948). (See Table I.)

We report in Table I the original data of the beginning of a typical run. They were taken with the following set-up:

Diameter of neutron beam exit hole was 2.22 cm.
Distance from exit hole to scatterer was approximately 350 cm.
Distance from scatterer to first counter was 85 cm.
Distance from scatterer to monitor was 140 cm.
Triple coincidence was used.
The scatterers measured 11 by 11 cm and were made of polyethylene and graphite.
The thickness of the scatterers and absorbers is indicated in Table I.

A word must be added on the measurements in the direction of the primary beam ($\Phi=0°$): The value of the cross section at $\Phi=0°$ was obtained with apparatus *A* using the same procedure as that used in measuring at $\Phi\neq0°$ but with some added precautions due to the fact that the primary neutron beam passed directly through the counters. The beam was stopped

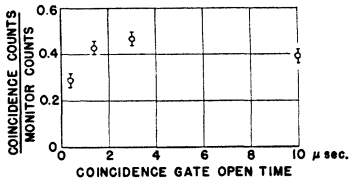

FIG. 6. Influence of the length of the gate open time on the coincidence counting rate.

down to an aperture 1.25 cm in diameter at the concrete shield and the intensity was reduced to about 3 percent of the usual operating intensity. The loss in intensity was partially compensated by using a thicker scattering target. The results obtained at 0° are given in Table II.

F. The Apparatus for $\Phi > 60°$

The apparatus schematically drawn in Fig. 2 was used for angles between 0 and 60°. At larger angles the thickness of the scatterer itself, the air, windows, etc., make this type of apparatus inadequate. A new apparatus shown in Figs. 7

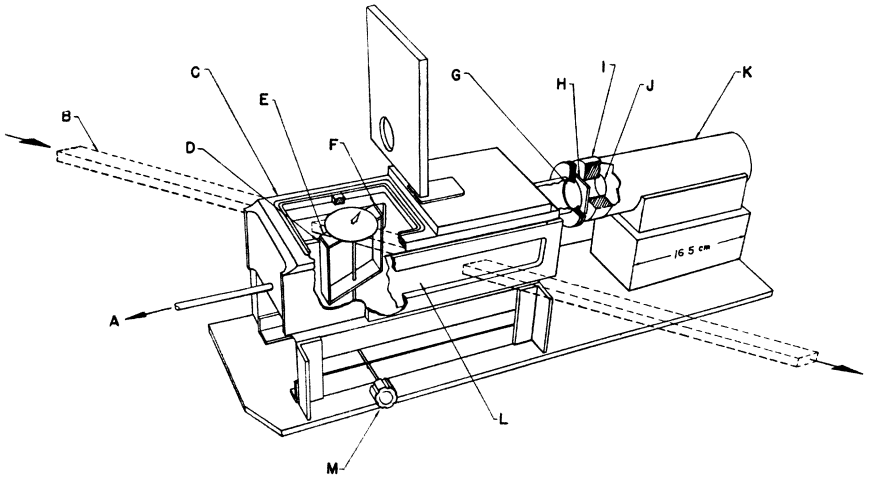

FIG. 7. Drawing of apparatus *C*.

A—to pump
B—neutron beam
C—vacuum scattering chamber
D—carbon scatterer
E—scatterer support
F—polyethylene scatterer
G—aluminum window
H—carbon absorber
I—diaphragm
J—mica window
K—counter telescope (four counters)
L—0.002-in. steel window
M—scatterer locator

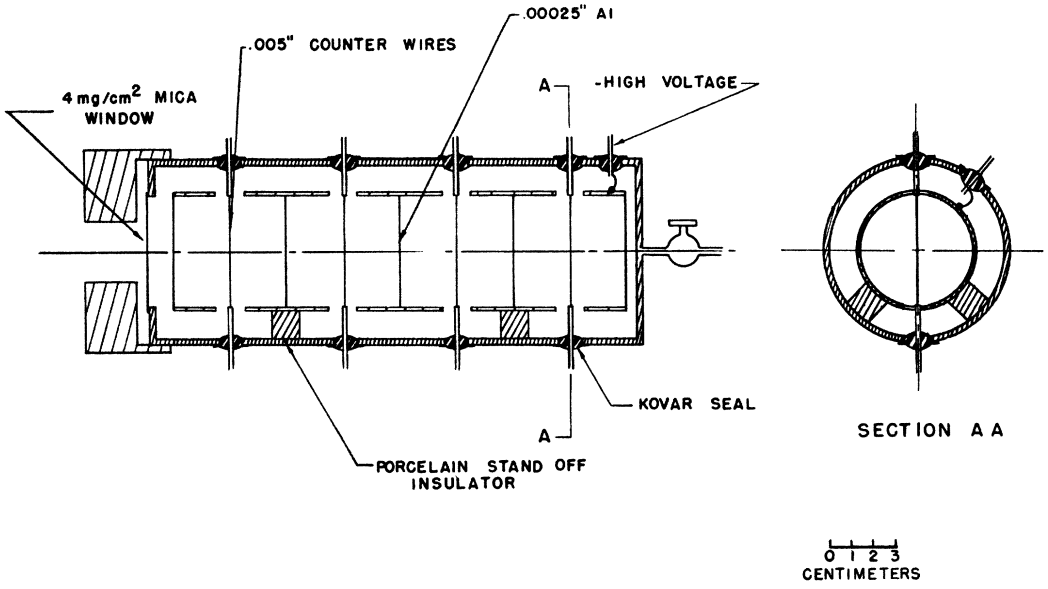

FIG. 7a. Detail of Fig. 7 counter telescope *K*.

TABLE III. 40-Mev $\sigma(\Phi)$ in 10^{-27} cm² per steradian. All runs have been fitted to the average of runs 2, 3, and 5.

Run number		1	2	3	4	5	6	7	8		
Symbol in Fig. 10		▼	○	●	□	○	△	×	▭		
Date		4-20-48	4-29-48	6-23-48	8-5-48	8-5-48	4-30-48	6-26-48	8-4-48		
Apparatus		*A*	*A*	*A*	*A*	*A*	*C*	*C*	*C*		
	Φ (deg.)									θ (deg.)	$\frac{d\cos\Phi}{d\cos\theta}$
	0				76.1±2.8					180	0.250
	5			68.1±2.2						170	0.251
	10	63.2±3.0	65.2±2.2	66.5±1.7	69.8±1.6	66.7±2.2				160	0.254
	15		53.2±5.4	62.1±1.7		59.3±2.2				150	0.258
	20		54.7±4.5	57.8±2.1	52.2±1.1	54.6±1.9				140	0.258
	25		52.2±4.7	55.0±1.6		49.2±1.9				130	0.276
	30	44.2±1.1	45.3±2.1	43.9±1.5		42.5±1.9				120	0.289
	35		39.4±2.9	40.8±1.6		39.8±1.9	35.4±2.3	39.4±1.6	38.9±1.6	110	0.306
	40		35.4±2.2	36.2±1.3		43.5±1.9				100	0.327
	45	34.6±2.6	35.9±2.2	30.2±0.9		36.2±1.9	36.5±1.9	32.5±1.2	33.0±1.6	90	0.354
	50						22.7±4.5		29.9±1.5	80	0.389
	55						28.5±1.8		25.2±1.2	70	0.435
	59						27.0±1.9	24.8±1.0	19.6±1.6	62	0.485

and 7a was built and was used to measure the scattering cross section for $35° \leq \Phi \leq 71.6°$. At larger angles all the difficulties introduced by matter in the path of the scattered beam and by the thickness of the scatterer become critical, and the rapidly increasing difficulty of the experiment made it impractical to exceed the angle of 71.6° with our present apparatus.

The apparatus shown in Fig. 7 relieved some of the difficulties mentioned above by providing for the evacuation of a space surrounding the scatterer and extending almost to the counter tube. Two benefits were obtained from this. First, the direct replacement of a 33-cm air column (equivalent to about 50 mg cm^{-2} Al) by an 11-mg cm^{-2} Al window and, second, the removal of the air from the beam path, which greatly decreased the background radiation. This fact in turn made it possible to use thinner scatterers (25-mg cm^{-2} CH_2), thus decreasing absorption within the scatterer.

The apparatus was made in the form of an aluminum alloy box, with 38-mg cm^{-2} rectangular stainless steel windows on opposite sides to allow passage of the beam. The arrangement provided for minimum production of protons by interaction of the beam with the box walls. On a third side was fixed an 11-mg/cm² aluminum window, through which the protons scattered by the target pass to reach the counting tubes. The carbon and polyethylene scatterers inside of the box were mounted on a rack which could be rotated from the outside to place either scatterer at a point within the beam and perpendicular to the axis of the counting tubes, or to place both out of the beam. A scale calibrated in degrees was attached to the rack, and a transparent window placed in the top of the box, so that the scatterers could be accurately placed for a run. The telescope of counting tubes was fixed permanently to the vacuum box, and adjustment to various scattering angles was made by rotating the entire apparatus on a pivot directly under the point occupied by the scatterer when in place for a run. The beam windows were made long enough to allow for this shifting of beam position with respect to the box. A removable cover was placed over the scatterers to provide access to them. Since there was no need to attain a very high degree of vacuum, no special precautions were necessary in making the box vacuum tight. It was evacuated by a small mechanical pump which ran continuously during the course of an experiment.

In order to decrease the amount of material in the path of the scattered protons all four tubes of the counting telescope were built into one envelope with resultant elimination of the windows between the individual units, as indicated in Fig. 7a. With this arrangement, of course, it was impossible to place absorbers between the last two tubes of the counting telescope. Consequently they had to be put in front of the whole telescope and the effect of Rutherford scattering by the absorber was somewhat more serious than in the other apparatus. This effect has been discussed under "*C*."

G. Lower Energy Experiments

By reducing the radius at which the beryllium probe is hit by the deuteron beam it is possible to obtain, by the stripping process, neutrons of lower energy. Unfortunately the width of the energy distribution in the forward direction does not decrease as much as the most probable energy, so that poorer energy resolution is obtained. This is born out in Fig. 8, where the theoretical neutron energy distribution is plotted for $E_D = 98$ Mev and a target of 1-cm beryllium. Be this as it may, we have repeated the experiments with the same apparatus at a lower energy. The results are reported in Table III and in Fig. 10.

H. Summary of All the Experimental Results

Tables II and III contain a summary of all the experimental results of this investigation thus far obtained on the angular dependence of np cross section.

It must be added that several authors have found that for energies lower than 15 Mev $\sigma(\vartheta)$ is independent of ϑ.

III. TOTAL CROSS-SECTION EXPERIMENTS

In order to place the measured cross sections on an absolute scale it is necessary to determine the total scattering cross section. This can be accomplished by an attenuation measurement of the neutron beam using good geometry. Actually in the experiments we measured

$$\int N(E)D(E)dE \tag{10}$$

and

$$\int N(E)D(E)\exp[-s\sigma_t(E)]dE, \tag{11}$$

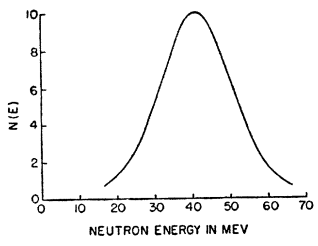

FIG. 8. Theoretical neutron energy distribution for stripping of 98-Mev deuteron on 1-cm thick beryllium. The neutrons are in the forward direction.

where $N(E)dE$ is the number of neutrons between energies E and $E+dE$ impinging on the absorber, $D(E)$ is the probability that one of these neutrons is counted by the special detector used, $\sigma_t(E)$ is the total cross section of the attenuator nuclei, and s is the number of nuclei per cm^2 of the attenuator. If the neutrons employed were monochromatic, $N(E)$ a delta-function, or if $D(E)$ were a delta-function, the ratio of (11) to (10) would immediately give $\sigma_t(E)$. Unfortunately, this is not the case and there is appreciable uncertainty in the interpretation of the attenuation measurements.

The experiments were performed using as attenuator a column of hydrocarbon (pentane, polyethylene, etc.) and also a column of graphite containing approximately the same amount of carbon as that in the hydrocarbon. The attenuation produced by each absorber under good geometry conditions was measured and from it the hydrogen cross section was deduced.

Typical geometrical conditions as shown by Fig. 9 were: diameter of neutron beam, 1.9 cm; length of absorber, 58 cm; cross section, 5×5 cm; distance between closest end of absorber and detector, 50 cm; diameter of detector, 4.4 cm.

Estimates of multiple scattering effects show them to be negligible.

In Table IV we report the main results thus far obtained.

We can estimate an effective average energy for the neutrons used and calculate $E_{\text{eff}}\sigma_t(E_{\text{eff}})$; we may expect the last quantity to be nearly constant. This is roughly the case if we assume a primary neutron distribution similar to that predicted by Serber plus a low energy tail of an amplitude of about 20 percent of the maximum extending down to 20 Mev, reasonable functions $D(E)$, and $\sigma_t(E)$ inversely proportional to E_n. The E_{eff} of Table IV have been calculated under these hypotheses.

In conclusion we can assume $\sigma_t = 6.85/E$ (E in Mev, σ_t in 10^{-24} cm^2) with about 10 percent uncertainty. This value does not match too well with the approximate values of $\sigma_t = 9.8/E$ reported by Sleator[7] on the basis of measurements in the 20- to 24-Mev energy interval; there is,

[7] W. Sleator, Jr., Phys. Rev. **72**, 207 (1947). See also for further bibliography.

however, no reason why $E\sigma_t(E)$ should be constant over such large energy intervals.

IV. CONCLUSION

In Tables II and III we give $\sigma(\Phi)$. In order to find the corresponding $\sigma(\theta)$ we have to multiply $\sigma(\Phi)$ by $d\cos\Omega/d\cos\theta$ and put this value at the angle θ corresponding to the Φ considered. Table II also gives θ and $d\cos\Phi/d\cos\theta$ as a function of Φ for 88 Mev. For 40 Mev, we have used the non-relativistic formulae

$$-\theta=\pi-2\Phi;\quad \frac{d\cos\Phi}{d\cos\theta}=\frac{1}{4\cos\Phi}.$$

The normalization of the curves is done as explained before by requiring that

$$\int\sigma(\theta)d\omega=\sigma_t=\begin{matrix}0.076\times10^{-24}\text{ cm}^2\text{ for 90 Mev}\\ 0.170\times10^{-24}\text{ cm}^2\text{ for 40 Mev.}\end{matrix}$$

Since $\sigma(\theta)$ is known only in a limited range, we have arbitrarily extrapolated $\sigma(\theta)$ in the unknown region in a way very close to curve I of Fig. 11. The contribution of this part of the curve to the total cross section is 15 percent of the total for the 90-Mev curve. The extrapolated part of the curve is also consistent with data obtained in the cloud-chamber investigation of n-p scattering by Bruckner *et. al.*[6] We have assumed the 40-Mev curve to be symmetrical around 90°.

The values of $\sigma(\theta)$ obtained in *all* runs are reproduced in Fig. 10. The stars are, in our judgment, the best average of the measurements we have at the present date; in drawing them we have weighted the experimental runs. For clarity it has been impossible to give the statistical errors which can be easily read out of Tables II and III. The spread of the points gives a fair over-all impression of the accuracy of the measurements.

Messrs. R. Christian and E. Hart of the theoretical group of the Radiation Laboratory have calculated the n-p cross sections under various assumptions.[8] One of the simplest used, which agrees fairly well with the experimental results, is the following.

The n-p scattering depends on a potential

$$V(r)=g^2(e/r)^{-Kr}(1+P/2),$$

where the constant g^2 has two values, one for scattering with parallel and the other with antiparallel spins. These values correspond to $g^2/\hbar c=0.405$ and 0.280, respectively, and are chosen so as to fit the scattering cross section for epithermal neutrons and the binding energy of the deuteron. The constant $1/K$ is $1.2\cdot10^{-13}$ cm. If we interpret $1/K$ as the "Compton wavelength" of a particle, this particle has the mass of 326 electronic masses which is not very different from the π-meson mass; moreover, this is the value of the range of the nuclear forces used by Breit in interpreting p-p scattering, and it also fits the coherent scattering observed in neutron scattering by ortho and parahydrogen. P is an

TABLE IV. Results of total cross-section measurements. ρl gives the thickness of absorber with which the measurements were taken. In runs 1, 2, 4, and 5 about 85 percent of the detected protons came from hydrogen recoils, the rest from carbon and background. In run 6 only protons coming from hydrogen recoils were taken into account. The approximate total cross section of carbon at 90 Mev is 0.53×10^{-24} cm² and at 40 Mev 0.93×10^{-24} cm².

Run no.	Absorber	ρl g cm^{-2}	Method of neutron detection	E_{eff} Mev	σ_t 10^{-24} cm²	$E\sigma_t$
1	Polyethylene	35.3	Protons from CH_2	40	0.177±0.010	7.08
2	Polyethylene	35.3	Protons from CH_2	40	0.154±0.015	6.16
3	Paraffin[a]		$C^{12}(n,2n)C^{11}$	78	0.083±0.004	6.47
4	Pentane	67.2	Protons from CH_2	88	0.075±0.010	6.60
5	Polyethylene	53.4	Protons from CH_2	88	0.086±0.010	7.56
6	Polyethylene	53.4	H recoils from CH_2	88	0.066±0.018	5.80
7	Pentane[b]	67.2	Fission of Bi	95	0.074±0.002	7.03
8	Polyethylene	53.4	Fission of Bi	95	0.062±0.007	5.89

[a] Cook, McMillan, Peterson, and Sewell, Phys. Rev. **72**, 1264 (1947).
[b] J. DeJuren, N. Knable, and B. J. Moyer, private communication.

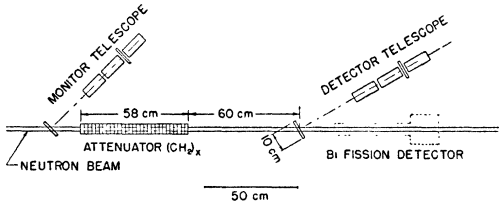

FIG. 9. Typical arrangement for measurement of the total scattering cross section.

[8] A review of the subject is given in L. Rosenfeld, *Nuclear Forces* (Interscience Publishers, Inc., New York, 1948). Other calculations on n-p high energy scattering: M. Camac and H. A. Bethe, Phys. Rev. **73**, 191 (1948); J. Ashkin and Ta-You Wu, Phys. Rev. **73**, 973 (1948).

operator that exchanges the spatial coordinates of neutron and proton.

The above potential gives an angular distribution as shown in Fig. 11, curve *I*, and a total cross section at 90 Mev of 0.090×10^{-24} cm^2. The agreement is fairly good and the simplicity of the hypotheses make this result attractive, although the theoretical total cross section is appreciably larger than the experimental one.

On the other hand, tensor forces must be

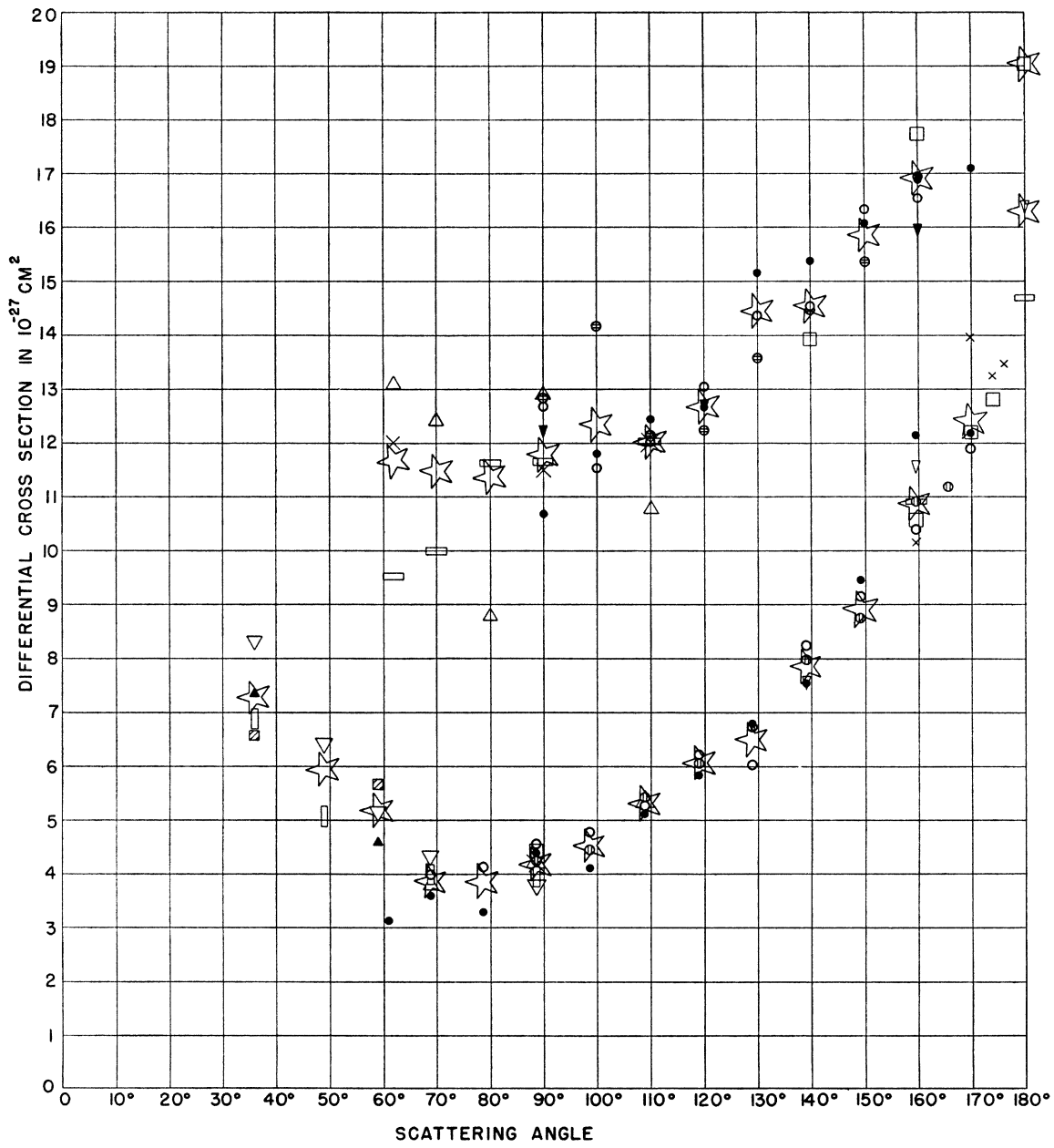

FIG. 10. Differential neutron proton cross section in the center of gravity system in 10^{-27} cm^2/steradians. All measurements are included (see key to symbols in Tables II and III). The stars are the final best available average corrected as described in the text. The upper curve represents the data taken with 40-Mev neutrons; the lower curve with 90-Mev neutrons.

present to account for the electric quadrupole moment of the deuteron and they can be introduced by changing the potential to

$$V'(r)=g^2\left\{\frac{e^{-Kr}}{r}+\gamma\left(\frac{3(\sigma_1\cdot r)(\sigma_2\cdot r)}{r^2}-\sigma_1\cdot\sigma_2\right)\frac{e^{-K'r}}{r}\right\}\frac{1+P}{2},$$

where σ_1, σ_2 are the spin operators, γ is a constant fixing the amount of tensor force and K' is the range of the tensor forces. Choosing $\gamma=0.16$ and $K'=0.3K$ it is possible to account for the electric quadrupole moment of the deuteron. However, the total cross section becomes even larger: 0.093×10^{-24} cm^2, and the angular distribution hardly agrees with the experimental one.

It must be remembered that relativistic effects have been neglected and they may be of the order of 20 percent.

More detailed theoretical studies to bring out the separate influences of the single factors involved in the *n-p* cross section are in progress.

The authors wish to thank Professor E. O. Lawrence for his interest in this work, and the cyclotron operating crew for their valuable assistance in making the runs.

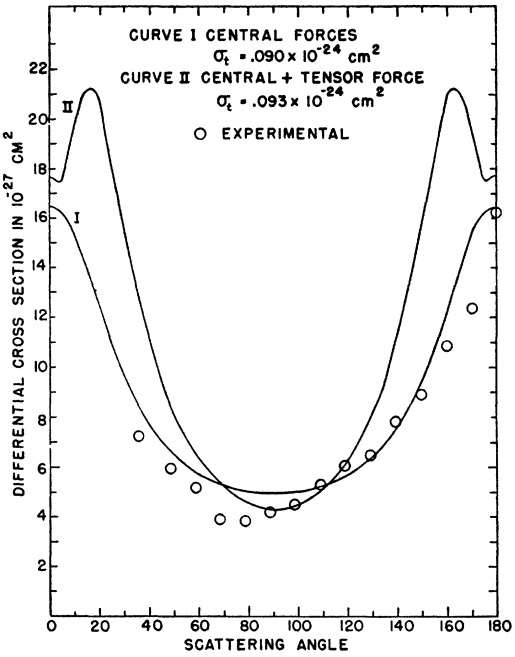

FIG. 11. Theoretical *n-p* scattering curves drawn according to the hypotheses discussed in the "Conclusions" section. Curve I central forces $\sigma=0.09\times10^{-24}$ cm^2; curve II tensor forces $\sigma_t=0.093\times10^{-24}$ cm^2. Circles are the experimental points.

This paper is based on work performed under the auspices of the Atomic Energy Commission.